

THE LATE-TYPE STELLAR CONTENT OF NGC 2403

By

J. DAN HUDON

B.Sc., The University of Calgary, 1986

**A THESIS SUBMITTED IN PARTIAL FULFILLMENT OF
THE REQUIREMENTS FOR THE DEGREE OF
MASTER OF SCIENCE**

in

THE FACULTY OF GRADUATE STUDIES

Department of Geophysics and Astronomy

**We accept this thesis as conforming
to the required standard**

THE UNIVERSITY OF BRITISH COLUMBIA

October 1988

© J. Dan Hudon, 1988

In presenting this thesis in partial fulfilment of the requirements for an advanced degree at the University of British Columbia, I agree that the Library shall make it freely available for reference and study. I further agree that permission for extensive copying of this thesis for scholarly purposes may be granted by the head of my department or by his or her representatives. It is understood that copying or publication of this thesis for financial gain shall not be allowed without my written permission.

Department of Geophysics & Astronomy
The University of British Columbia
Vancouver, Canada

Date Oct 17 / 88

Abstract

We have examined the late-type stellar content of 3 disk fields of NGC 2403 using VRI CCD photometry. The AGB luminosity function has been constructed and differs strongly with that of the LMC. Notably, even fewer bright AGB stars are seen in NGC 2403 than in the LMC. The shape of the AGB luminosity function for the innermost field, however, indicates that a recent burst of star formation may have occurred. Red and blue supergiants and HII regions are also identified in the field to support this. The relative distance modulus between NGC 2403 and the LMC is derived to be 8.90 and the true distance modulus to NGC 2403 is $(m - M)_0 = 27.40 \pm 0.24$. The carbon to M star number for the innermost field is 8/17 which corresponds to $[Fe/H] = -0.35$.

Contents

Abstract	ii
List of Tables	v
List of Figures	vi
Acknowledgements	vii
1 Introduction	1
2 Observations and Data Reduction	3
2.1 The Data	3
2.2 DAOPHOT	8
2.2.1 Reduction	8
2.2.2 Completeness	10
2.3 Photometry of Standard Stars	15
3 The Color-Magnitude Diagrams	20
4 The AGB Luminosity Function	24
4.1 Introduction	24
4.2 The Bolometric Magnitude-Color Diagrams	25
4.3 Completeness and the Luminosity Function	30

5	The Distance to NGC 2403	40
6	The C and M Star Study	46
6.1	The Photometric Method	46
6.2	The Color-Color Diagram	47
7	Summary	53
	References	55

List of Tables

1	Log of Observations for NGC 2403	5
2	Results of Completeness Tests	13
3	Observations of Standard Stars	18
4	AGB Luminosity Functions	35
5	Cepheid Observations in NGC 2403	43
6	Summary of P-L fits	44
7	C and M stars in NGC 2403	50

List of Figures

1	The Three Fields studied in NGC 2403	6
2	I photometry errors of artificially added stars	14
3	Transformations for Standard Stars	19
4	Color-Magnitude Diagram for Field 1	22
5	Color-Magnitude Diagrams for Fields 2 and 3	23
6	Bolometric Magnitude-Color Diagram	28
7	Color - Bolometric Magnitude Diagram	29
8	Completeness Curves for color and M(bol)	36
9	Bolometric Luminosity Function for Field 1	37
10	Bolometric Luminosity Function for Fields 2 and 3	38
11	Corrected and Uncorrected luminosity functions	39
12	Period-Luminosity relation for LMC Cepheids	45
13	The Narrowband Filters	51
14	The (81-78) , (R-I) color-color diagram	52

Acknowledgements I would like to thank my supervisor Harvey Richer for his patience and support during this project. Several people provided additional assistance over the course of the past two years: in particular, thanks to: Greg Fahlman and Paul Hickson for several informative discussions; Gerry Grieve and Dan Hurley for help with programs; Carol Christian at CFHT for readily supplying the outer fields; and Jaymie Matthews and Jim Nemec for careful readings of early drafts of this thesis. Thanks also to Kavan Ratnatunga for supplying foreground star counts. And special thanks to my family and friends who have encouraged me all along.

1 Introduction

Studies of the stellar content of nearby resolved galaxies have become increasingly viable in recent years. With the advent of CCDs and improved data reduction techniques the stars of more distant galaxies can be observed to fainter limits.

Until the early 1980's, extra-galactic studies of luminous asymptotic giant branch (AGB) stars had been confined to the nearby Magellanic Clouds and the sparse dwarf spheroidals surrounding the galaxy (see Aaronson 1983, 1986). The rewards of these surveys have been rich. In particular, the estimation of absolute magnitudes of carbon stars (hereafter, C stars), C star luminosity functions, the C-to-M star number ratio and the estimation of the ages of globular clusters in the SMC and the LMC, each of which has provided strong constraints on the evolutionary theory of intermediate mass stars.

CCD studies of late-type stars in other Local Group galaxies began in earnest in the mid-1980's by groups led by Richer (see Richer, *et al.* 1984) and by the late Marc Aaronson (see Cook, Aaronson and Norris 1986, hereafter CAN86). Both groups adopted a simple narrowband photometric technique for the identification of C and M stars. The primary results of these programs are as follows: (1) they have uncovered a fairly strong correlation between the C/M ratio and metallicity, (2) they have supplied C star and AGB luminosity functions in differing galactic environments, and (3) they have shown that carbon stars can be useful as distance indicators out to ~ 4 Mpc.

This thesis presents observations of AGB stars in NGC 2403, the most distant galaxy in which AGB stars have been observed and probably at the limit for ground based studies. NGC 2403 is a late-type spiral of type Sc(s) III (Sandage and Tammann 1981) and is associated with the M81 group of galaxies. Previous stellar content studies of NGC 2403 by Tammann and Sandage (1968) and Sandage (1984) were primarily examinations of the brightest red and blue variables for distance determinations.

The late-type stars that are treated in this thesis occupy the upper-AGB with bolometric magnitudes in the range $-7.2 \leq M_{bol} \leq -4.0$ and have $(R - I)_o > 0.75$. They are predominantly C stars, which are defined to have a surface abundance of $C > O$ (Iben 1983), and M stars ($C < O$). Section 2 describes the observations and reduction of the data. In Section 3, the color-magnitude diagrams for the fields observed in NGC 2403 are discussed. Section 4 is devoted to the AGB luminosity function and its completeness corrections. In Section 5, the distance to NGC 2403 is derived, based on random-phase I-band observations of Cepheids. The C and M star study using the narrowband photometric technique is presented in Section 6. Finally, Section 7 summarizes the key results of this thesis.

2 Observations and Data Reduction

2.1 The Data

The data were obtained by Chris Pritchett and Dennis Crabtree at the Canada-France-Hawaii 3.6m Telescope (CFHT) between Feb. 7 and 11, 1986, using an RCA CCD camera (320 x 512 pixels) at the Cassegrain focus. In this configuration, the scale on the detector is $0.22''$ per pixel. The observations consisted of CCD frames of a single field in the disk of NGC 2403, through each of four filters (2 wide-band and 2 narrow-band). The field is located approximately $170''$ from the nucleus or 2.5 kpc (assuming a true distance modulus of 27.4, see Section 5), and measures $70'' \times 110''$ or $1.6 \text{ kpc} \times 1.0 \text{ kpc}$.

The broad-band filters were chosen to approximate the Cousins I and R filters (Bessell 1979). Additional I and V frames of two fields containing Cepheid were also available, the data obtained during Director's discretionary time at CFHT during December, 1985. These fields are located at $360''$ (5.0 kpc) and $480''$ (6.6 kpc) from the nucleus. The log of the observations is summarized in Table 1. The location of the 3 fields in NGC 2403 and the position of the CCD chip is shown in Figure 1.

All preprocessing of the frames was done at CFHT. This involved subtracting dark frames of equal exposure times to the program frames, dividing out flat-field exposures taken of an area of the dome that was uniformly illuminated and 'defringing' (see below). Seeing was $1.0''$ or better for all exposures except for the narrowband 8100

Å frame where the seeing is $1''.3$. Thus, it is this frame which limits the carbon and M star study of Field 1. Although frames were taken through each filter during the Feb. 1986 run, the image quality was noticeably worsened when they were averaged together, therefore, only that frame with the best seeing was analysed.

CCD images are often subject to optical fringing, particularly in the infrared, due to interference effects in the thin silicon layer on the surface of the chip (Walker 1987). In general, a 'flat' field image, in which the chip is uniformly illuminated in some manner, is used to remove the fringes. For these observations, flat-field exposures were taken of a dark patch of the sky. All of the Field 1 frames were successfully defringed except for the 7750 Å exposure. However, the degree of fringing on this frame did not appear severe enough to seriously affect the photometry. The fringing patterns evident on the I-band frames of Fields 2 and 3 were removed by scaling and subtracting an I fringe frame taken during the Feb. 1986 run (using routines in the LIPS package at UBC (Grieve 1984)).

Table 1: Log of Observations for NGC 2403

Date	Filter	Exp. (sec)	Seeing (FWHM) ^b	Designation	Cepheids ^a
1986 Feb.7-11	I	2400	0".8	Field 1	v4
	R	2400	1".0	Field 1	v4
	7750	2400	1".0	Field 1	v4
	8100	2400	1".3	Field 1	v4
1985 Dec.15-16	I	1800	0".9	Field 2	v40,v42,v46
	V	1800	0".8	Field 2	v40,v42,v46
1985 Dec.15-16	I	1800	0".9	Field 3	v3
	V	1800	0".9	Field 3	v3

^arefer to Tammann and Sandage, 1968.

^bFWHM = $2.355\sigma_{PSF}$, see DAOPHOT manual.

Figure 1: See photograph, next page. The fields are also identified by the Cepheids found in each (Tammann and Sandage 1968). Refer to Table 1.

2.2 DAOPHOT

2.2.1 Reduction

Stellar photometry involves measuring the apparent brightnesses of stars in a given wavelength region. Ideally, one would isolate the star within an aperture large enough to include the entire seeing disk, then integrate the intensity over the area of the aperture and subtract from this the contribution of the sky background. In crowded fields, however, large apertures can be severely contaminated with the light from neighboring stars, making it difficult to make reliable brightness measurements for any individual star. In response to this, Stetson (1987) developed the point-spread function fitting package DAOPHOT. (A point-spread function (PSF) is the two-dimensional brightness distribution produced by the image of the star on the detector (Stetson 1987)). Here, a PSF, derived from stars on the the frame, is shifted and scaled to each individual star in its group; the apparent brightnesses are obtained when the residuals of the fit (to the entire group) are minimized. In this way, a complete set of *relative* magnitudes is estimated for all the stars on the frame.

The reduction procedure adopted for this study was similar to that suggested in the DAOPHOT manual. A brief outline follows. Stars were recognized by the FIND routine as statistical fluctuations above the average background noise level. The FIND threshold was set to detect fluctuations at a level of 3σ or greater. This threshold was raised to 4σ and 5σ for the R and I (Field 1) frames in an effort to improve the

confidence in detection. Aperture photometry (the PHOT routine) is then performed on the resulting star list using an aperture with a radius of the order of the FWHM (in pixels) for the frame. The “best” stars, which are isolated but not necessarily the brightest, were used to construct the PSF. Two or three iterations were required to remove the neighbors of the PSF stars and the final PSF contained a minimum of 3 stars.

The GROUP routine ensures that stars that are near each other are fit as a group, apart from the rest of the frame. The critical separation, which determines the size of a group, was nominally set to approximately twice the FWHM for a stellar image on the frame.

The PSF was scaled to the pixels within a “fitting radius” typically set to 0.5 pixels less than the FWHM. Both the errors in the photometry and the number of iterations required to reduce each group are sensitive to this fitting radius so it is important to test a few groups before reducing the entire frame.

The star list from the multiple-star PSF-fitting NSTAR routine is then subtracted from the frame and another pass is made to find the fainter stars that were missed the first time. A second NSTAR list from photometry on the subtracted frame is produced, the two lists are appended, grouped, and run through the NSTAR routine again. The final star list is thus the result of three NSTAR iterations and contains both the first pass and second pass stars in their appropriate groups.

This was the reduction procedure for the frames of Fields 2 and 3. Because of the proximity of Field 1 to the galactic nucleus, a gradient of unresolved stars existed across those frames. We removed this gradient to reduce systematic errors in the photometry by “flattening” the backgrounds of the Field 1 frames in the following manner (Pritchett *et al.* 1987). A subtracted frame (i.e., without stars) was created from the above final star list. Routines in LIPS were used to shift this background frame 7 pixels in each of 4 orthogonal directions, and smooth it using a boxcar of 5 pixels x 5 pixels, producing 4 new frames. The median of the 5 frames was taken and this, in turn, was subtracted from the original frame. Finally, a constant was added to bring the background back up to the original level, and DAOPHOT was run again, beginning from the FIND routine. This procedure did not change the small-scale fluctuations of the background, it only removed the large-scale gradient. The new NSTAR list did show improved photometric errors, probably because DAOPHOT implicitly assumes a constant sky background rather than a sky gradient.

Objects that had anomalously high errors for their magnitudes or large fitting errors of the PSF to the stellar group ($\chi^2 > 2.0$, where χ^2 is one of the fitting parameters returned by NSTAR) were eliminated from the star lists.

2.2.2 Completeness

Crowding of stellar images on a frame affects not only the errors in the photometry

but the “depth” of the photometry as well (i.e., the limiting magnitude for detection). To determine the completeness of the photometry as a function of magnitude, artificial stars of known magnitude were added into each frame using the ADDSTAR routine in DAOPHOT. These stars had the same profile as the point-spread function. The frame was then reduced as before. The fraction of the added stars that are recovered in a magnitude bin gives the completeness for that bin. The procedure was to add only a few stars at a time so as not to change the crowding statistics on the frame. This number was usually about 10 per cent of the total number in the frame’s NSTAR list. Several ADDSTAR tests were then run to improve the recovery statistics.

One of the problems with this procedure is that test stars are often recovered in a magnitude bin other than the one in which they are added. This is most severe for the faint artificial stars which are easily contaminated by nearby bright stars or positive noise fluctuations. Such “bin-jumping” has been treated rigourously in some recent papers by Drukier *et al.* (1988) and Stetson and Harris (1988). Here, however, a simpler approach was taken. Stars that were recovered in a bin 1.5 magnitudes or more from their original bin were considered spurious and deleted from the test. From 11 to 17 artificial star frames were created for each program frame. Fewer stars were added at the bright end because the photometry is virtually complete for the brightest bins but several hundred stars were added into the faint bins so that at least 100 stars were recovered in a bin and the Poisson error in the completeness fraction

is thus $\leq 10\%$. The results of the ADDSTAR tests for the I-band frame of Field 1 are shown in in Figure 2. In the figure, a bias in $\Delta I = I_{\text{recovered}} - I_{\text{added}}$ is evident fainter than $I = 23$. The completeness fractions for each frame are tabulated in Table 2.

Table 2: Results of Completeness Tests

Magnitude	$\Lambda_I (N_{\text{add}}, N_{\text{rec}})^a$	$\Lambda_R (N_{\text{add}}, N_{\text{rec}})$
Field 1		
18.0-18.5	1.00 (12, 12)	1.00 (10, 10)
18.5-19.0	1.00 (14, 14)	1.00 (10, 10)
19.0-19.5	0.91 (44, 40)	1.00 (12, 12)
19.5-20.0	0.96 (57, 55)	1.00 (12, 12)
20.0-20.5	0.95 (87, 83)	0.97 (33, 32)
20.5-21.0	0.99 (217,214)	0.95 (56, 53)
21.0-21.5	0.96 (352,339)	0.97 (119,123)
21.5-22.0	0.93 (311,290)	0.98 (177,181)
22.0-22.5	0.79 (364,289)	0.88 (259,228)
22.5-23.0	0.53 (386,206)	0.81 (333,269)
23.0-23.5	0.25 (322, 82)	0.54 (346,186)
23.5-24.0	0.13 (127, 17)	0.28 (319, 90)
24.0-24.5	...	0.13 (340, 44)
24.5-25.0	...	0.06 (258, 15)
	Λ_I	Λ_V
Field 2		
20.0-21.0	1.00 (61, 61)	1.00 (10, 10)
21.0-22.0	0.98 (179,175)	1.00 (10, 10)
22.0-23.0	0.96 (358,345)	1.00 (10, 10)
23.0-24.0	0.82 (279,229)	0.92 (199,215)
24.0-25.0	0.30 (64, 19)	0.60 (373,224)
25.0-26.0	...	0.13 (329, 43)
Field 3		
20.0-21.0	1.00 (22, 22)	1.00 (10, 10)
21.0-22.0	0.98 (132,134)	0.95 (20, 19)
22.0-23.0	0.94 (116,109)	0.95 (41, 39)
23.0-24.0	0.71 (228,162)	0.86 (212,182)
24.0-25.0	0.33 (286, 95)	0.43 (258,111)
25.0-26.0	...	0.14 (160, 22)

^a $\Lambda_F = N_{\text{rec}}/N_{\text{add}}$ is the completeness factor for filter F, N_{add} is the total number of artificial stars added in the bin and N_{rec} is the number recovered by DAOPHOT.

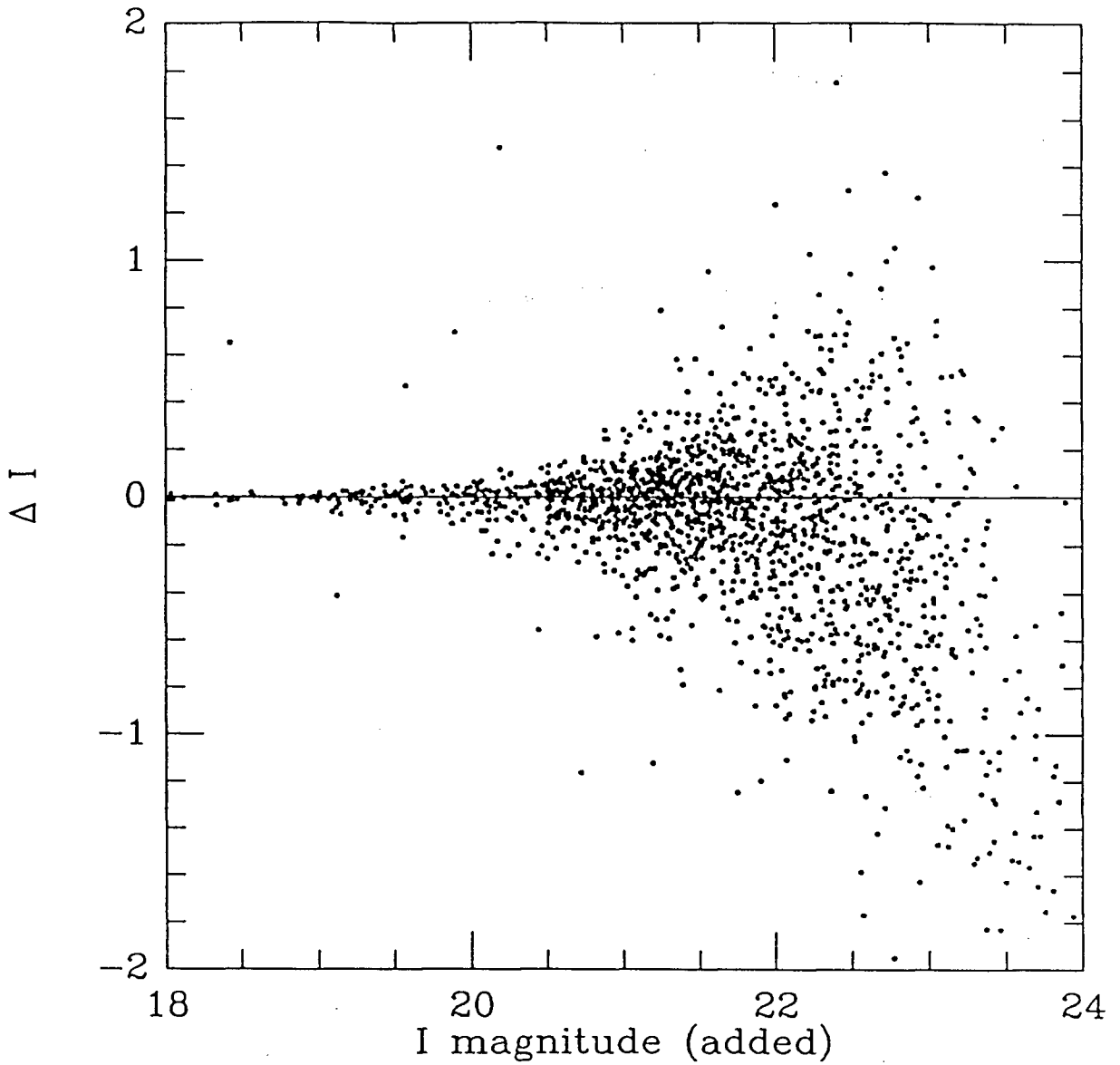


Figure 2: Results of the ADDSTAR tests for the I frame of Field 1. $\Delta I = I_{\text{recovered}} - I_{\text{added}}$ is plotted as a function of I_{added} . The tendency of faint artificial stars to be recovered at brighter magnitudes is evident.

2.3 Photometry of Standard Stars

The relative magnitudes on each frame were calibrated using short exposures of 12 CCD standards from nearby, uncrowded clusters (Schild 1983 and Christian et al. 1985). The standards were measured using large aperture-photometry and standard CFH extinction coefficients. The standards ranged in magnitude from 11.6 to 17.0 and in color from $(R - I) = 0.0$ to 0.8 so that some extrapolation of the color term was necessary for the reddest program stars.

The calibration procedure involved scaling all the standards to the same exposure time and correcting them for extinction. Magnitudes for the standards were derived for concentric apertures with radii ranging from 2 to 20 pixels. Plots were then made of magnitude as a function of aperture radius to see whether all the light of the star was being measured, ie. whether the curve was asymptotic at large apertures. Stars that had flat curves out to large apertures were chosen as primary standards. These were used to find an average aperture correction for the magnitude between an aperture of 10 pixels and one of 20 pixels radius. This number was of the order of 0.5%. The remaining standards were then measured at an aperture radius of 10 pixels and the aperture correction was applied to get the large aperture (20 pixels radius) magnitude.

The calibration equations have the form:

$$(R - I) = \mu(r - i)_0 + \zeta_{ri} \quad (1)$$

$$I - i_0 = \epsilon(R - I) + \zeta_i \quad (2)$$

where i_0 , $(r - i)_0$ are the instrumental magnitudes and colors corrected for extinction; I , $(R - I)$ are the standard magnitudes and colors taken from Schild (1983) and Christian et al. (1985); μ and ϵ are the slopes of the fitting relations and, ζ_{ri} and ζ_i are constants.

For the least-squares fit, equation 1 was rewritten in differential form (see Henden and Kaitchuck, 1982):

$$(R - I) - (r - i)_0 = (1 - 1/\mu)(R - I) + \zeta_{ri}/\mu \quad (3)$$

to give a more accurate error determination. The least-squares fits are shown in Figure 3.

The results for the color equation (3) were:

$$\mu = 1.553 \pm 0.080 \quad (4)$$

$$\zeta_{ri} = -0.454 \pm 0.032 \quad (5)$$

and for the magnitude equation (2):

$$\epsilon = 0.024 \pm 0.043 \quad (6)$$

$$\zeta_i = -4.985 \pm 0.018. \quad (7)$$

The slope in the magnitude equation (2) indicates a weak color term and the large slope in the color equation (3) is probably due to the fact that the R filter that was used was nonstandard.

In DAOPHOT, the NSTAR routine gives a relative set of magnitudes for all stars, the values of which depend on the PSF profile (and hence, the seeing) and the fitting radius used. For the calibration then, a least-squares relation between NSTAR photometry and aperture photometry was derived by measuring several bright stars using each method. For the I-band fits, the slopes were almost identically 1.000; the color fits had slopes that differed slightly from unity but the small errors indicate that this is probably random scatter. The final transformation equations for NSTAR magnitudes and colors to the Cousins system are:

$$(R - I) = 1.593(r - i)_{NSTAR} - 0.421 \quad (8)$$

$$I - i_{NSTAR} = 0.024(R - I) - 0.284. \quad (9)$$

Table 3: Observations of Standard Stars

Star	i	I - i	(r - i)	(R - I)
M92:				
8	21.446	-5.017	0.284	-0.047
100	20.579	-5.019	0.733	0.659
M67:				
106	17.398	-4.955	0.507	0.309
117	16.758	-4.993	0.554	0.442
124	16.581	-4.999	0.428	0.276
127	17.098	-4.954	0.479	0.334
128	17.467	-4.980	0.523	0.345
129	17.457	-4.975	0.544	0.375
130	17.321	-4.965	0.480	0.293
134	16.566	-4.963	0.531	0.344
NGC 2419:				
P	19.764	-4.931	0.522	0.350
Z	20.462	-4.953	0.770	0.734

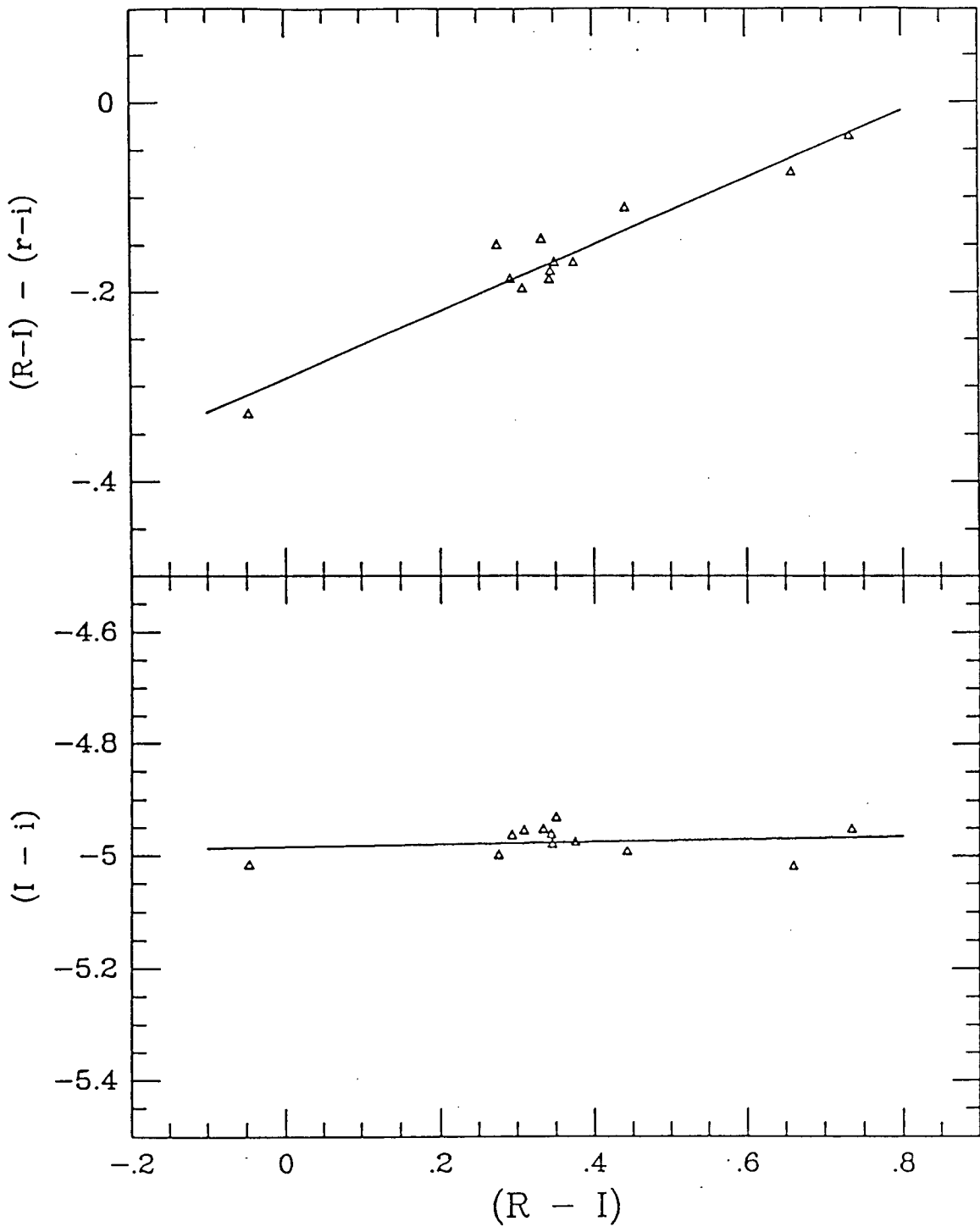


Figure 3: Transformations from the instrumental (ri) colors and magnitudes to the standard Cousins (RI) system. The equations for the two fitted lines are given in the text.

3 The Color-Magnitude Diagrams

The (I , $R - I$) color-magnitude diagram (CMD) for the innermost field (Field 1) is shown in Figure 4. Stars on the I and R lists (provided by DAOPHOT) were paired with a matching radius of 1.5 pixels resulting in 1015 matches or approximately 2/3 of each star list. There are several red and blue supergiant candidates with $I \leq 21.0$ in the diagram (reaching $M_I = -9.4$ for a distance modulus of 27.4, see § 5). Sandage (1984) and Humphreys (1986) have both observed red and blue supergiants in NGC 2403 at this magnitude or brighter, indicating that the most luminous stars seen in Figure 4 are all plausible members of NGC 2403. The number of blue supergiants is not very surprising because the CCD frame for this field does show several HII regions, indicating recent star formation. Although the foreground star contribution is expected to be negligible for this field (see below), it is still possible that some of these stars may be foreground red or white dwarfs.

Completeness in I drops below the 50% level at a magnitude of approximately 22.5 (Table 2), and this is evident in the CMD. The tip of giant branch of M92 (Mould, Kristian and Da Costa 1983), for example, appears at approximately $I = 23.4$, well below the completeness limit.

The distribution of foreground stars in the direction of NGC 2403 has been calculated for this field from the standard IAS-Galaxy model (Bahcall *et al.* 1987 and Ratnatunga 1988). That model predicts that the foreground star density is negligible

in this direction.

The $(I, V - I)$ color-magnitude diagrams for Fields 2 and 3 are presented in Figure 5. Frames for these fields were all shorter exposures than those for Field 1 (see Table 1). Both fields are located out in the disk (see Figure 1) and are quite sparse. However, more faint stars are visible in these fields than in Field 1 (compare Figures 5 and 4). There are 2 stars with I magnitudes brighter than 16.5 on the CMD for Field 3; these are probably foreground stars. Some blue and red supergiants candidates are seen on the CMDs of Fields 2 and 3 as well. Main-sequence stars are expected to have $(V - I) < 0.0$ (Reid, Mould and Thompson 1987); only a handful of stars brighter than I magnitude of 24 are seen in this color range.

Extinction within the galaxy NGC 2403 has not been estimated, thus, I magnitudes quoted here must be regarded as upper limits.

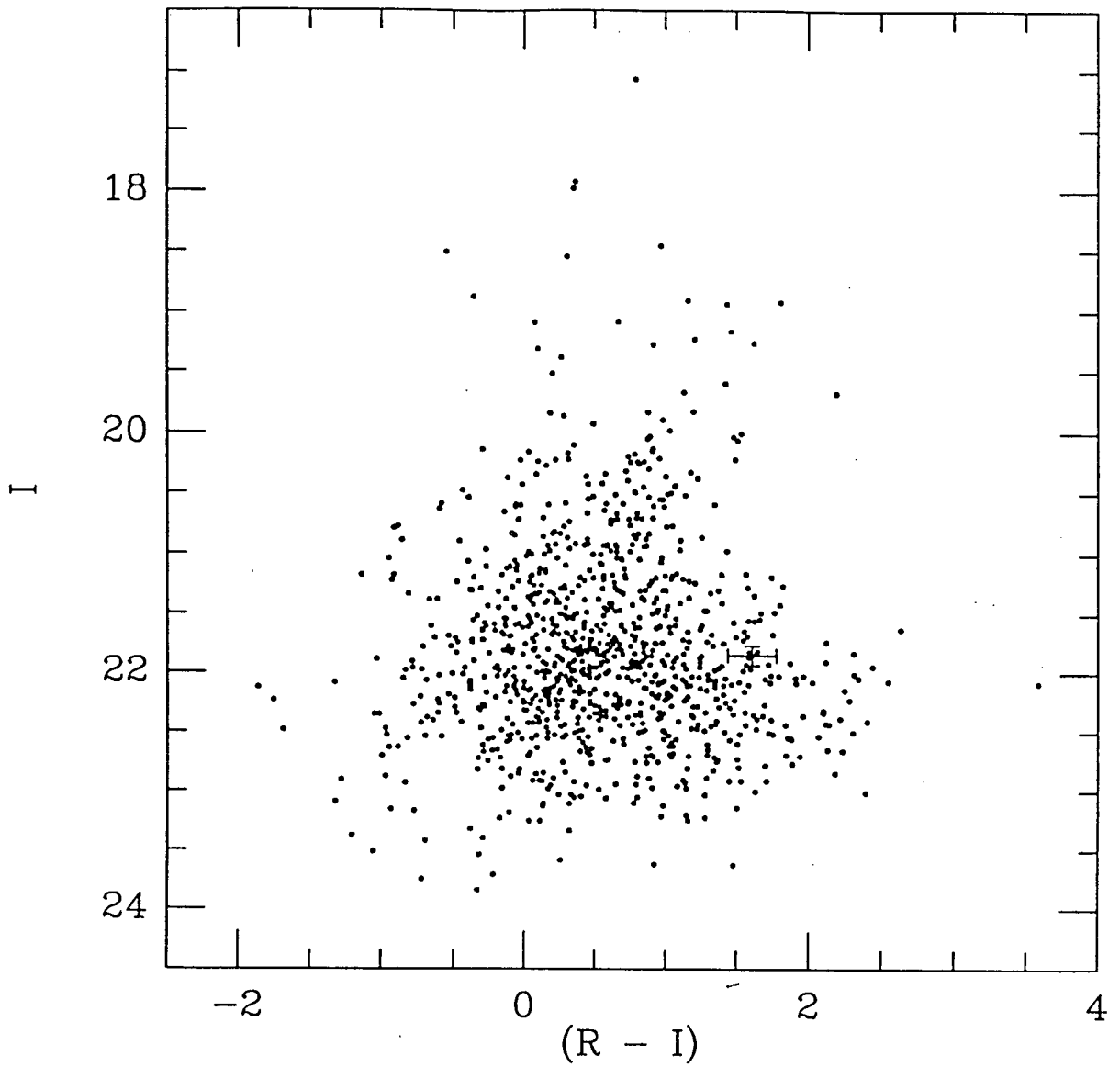


Figure 4: Color-magnitude diagram for Field 1. Typical errors in magnitude and color are indicated by the error bar.

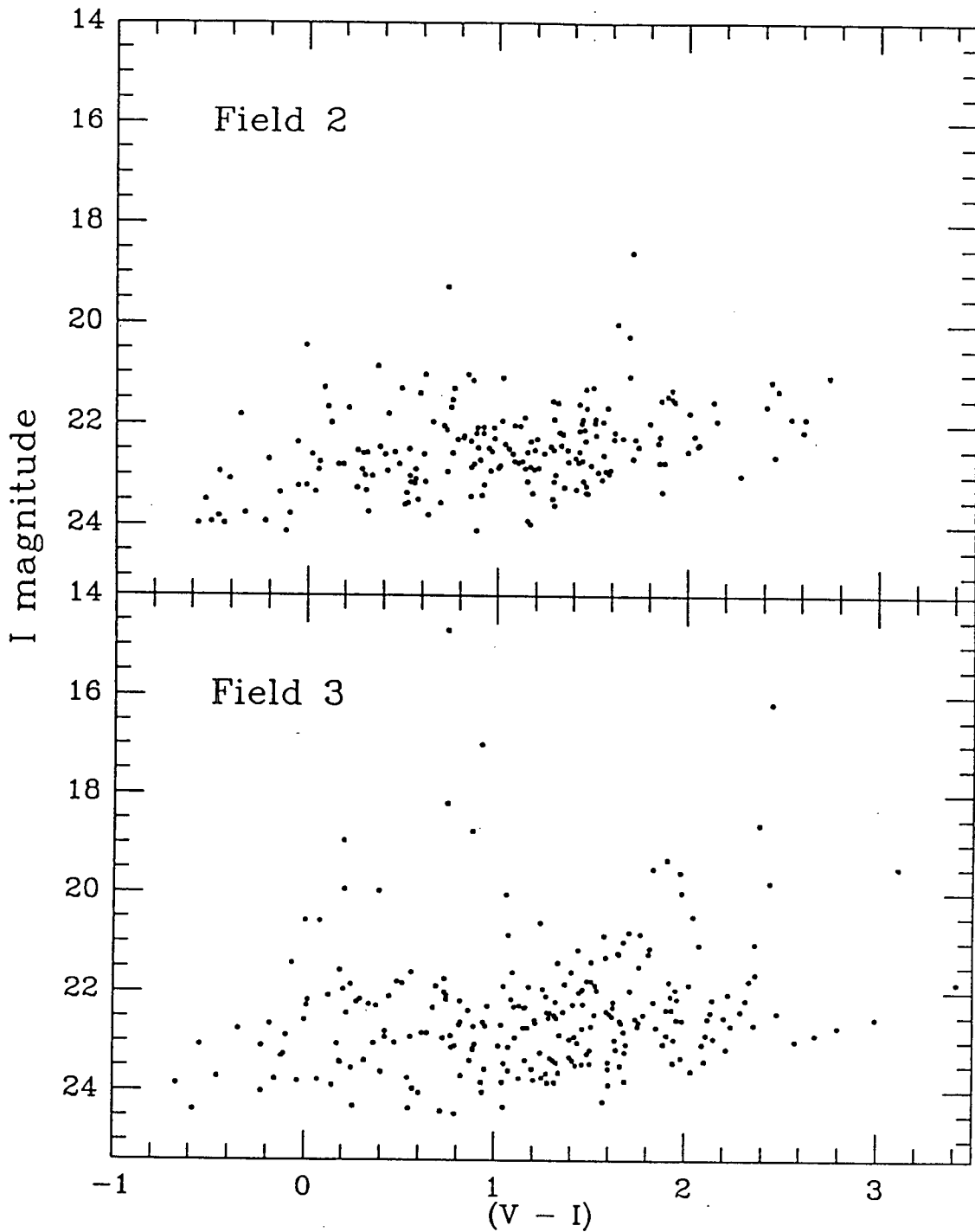


Figure 5: The $(I, V-I)$ CMDs for Fields 2 and 3 are shown here. There are approximately 220 stars in each. Note the morphological similarity in the two diagrams.

4 The AGB Luminosity Function

4.1 Introduction

The luminosity function for an ensemble of stars has long served as a tool to help understand stellar populations. In general, the luminosity function can be used to derive the initial mass function (IMF) which is one of the key parameters involved in the study of galaxy formation. It can also give important clues to the star formation history of the galaxy in question. For the AGB, the luminosity function also provides important constraints to the evolutionary theory, in particular, the effects of mass-loss, opacity, and convection.

A timely review of the observed AGB luminosity function in external galaxies is given by Richer (1988). Briefly, the situation is that the luminosity functions measured for fields in external galaxies show a pronounced deficit of bright AGB stars compared to current theoretical models. The problem was originally identified for C stars only (Frogel *et al.* 1981, Richer 1981) but a recent and extensive study of the LMC by Reid and Mould (1984), hereafter RM84, has demonstrated that the deficit applies to AGB stars of all types. Richer and his collaborators (see Pritchett *et al.* [1987] and references therein) have obtained similar results for fields in NGC 300, M31 and NGC 55. Several reasons for this disagreement between observation and theory have been suggested in the literature (cf. Iben 1981) but the currently favored explanation is that mass-loss on the AGB has been grossly underestimated. On the other hand,

Chiosi (see Chiosi (1985) and references therein) argues that convective overshooting needs to be accounted for in the models to produce valid results. Lattanzio (1988) discusses recent improvements in models of asymptotic giant branch stars. Mould (1983) has pointed out that since the theoretical AGB luminosity function involves three key pieces of information: (1) the star formation rate, (2) the IMF and (3) the mass loss rate of AGB stars, it is difficult to know where the problem lies. Therefore, it is the task of the observational astronomer to secure observations of AGB stars in several different galactic environments so that the theoreticians may fine tune the input parameters and adjust the models, thus promoting a better understanding of the details of stellar evolution at the tip of the AGB.

Before presenting the AGB luminosity function for NGC 2403, we first discuss the bolometric corrections and the completeness corrections that were applied to the data.

4.2 The Bolometric Magnitude-Color Diagrams

Bolometric corrections to the I magnitude were taken from Bessell and Wood (1984) where they derive corrections specifically for late-type stars. They give separate relations for both Cousins ($V - I$) and ($R - I$) indices. It should be noted that the scatter for their ($V - I$) relation is much smaller than that for the ($R - I$) relation and that carbon stars do not appear to fit either relation. RM84 derived their luminosity

function using a different bolometric correction (Mould, Kristian and Da Costa 1983), calibrated via globular cluster giants to a limit of $(V-I) = 2$. This luminosity function was also derived using the more recent bolometric corrections of Bessell and Wood (1984). Only minor differences were found between the two luminosity functions.

The galactic reddening in the direction of NGC 2403 was taken as $E(B - V) = 0.06$ (Tammann and Sandage 1968). This was converted to $E(R - I) = 0.05$ and $E(V - I) = 0.08$ using the reddening curve of Savage and Mathis (1979). Then, using a distance modulus of 27.4 (see § 5) the absolute bolometric magnitude equations become:

$$M(bol) = I + 0.1 + 1.09(R - I - 0.05) - 0.66(R - I - 0.05)^2 - 27.4 \quad (10)$$

and

$$M(bol) = I + 0.3 + 0.38(V - I - 0.08) - 0.14(V - I - 0.08)^2 - 27.4. \quad (11)$$

Errors in these equations are primarily due to the uncertainty in the distance which is estimated to be 0.25 magnitudes (see § 5). Internal reddening may also contribute.

The bolometric magnitude-color diagram from which the AGB luminosity function is derived is shown in Figure 6. Upper-AGB stars have bolometric magnitudes between ~ -4.0 and ~ -7.2 and become redder with increasing brightness. As seen in Figure 6, this sequence is quite well defined with the number of stars decreasing at higher luminosities. This effect may be due to the incompleteness of the sample for the reddest stars. (see § 4.3). The figure also shows a number of bright stars

that do not fall on the locus of the AGB. These very luminous stars are probably early M supergiants and are excluded from the AGB luminosity function. Although there are several differences in stellar structure between AGB stars and supergiants (Wood, Bessell and Fox 1983), observationally, we must rely on the fact that supergiants are brighter than AGB stars of the same color. A sequence of early M supergiants, adapted from Lee (1970) is included in the figure for comparison. Figure 6 demonstrates that the color criterion alone used by RM84 is inadequate to clearly distinguish the AGB stars from other bright stars. Hence, an upper limit to the AGB region was defined according to the morphology of the color-magnitude diagram and the location of the Lee supergiants in that diagram to make this distinction. Similar diagrams for the other two fields used in this study are shown in Figure 7.

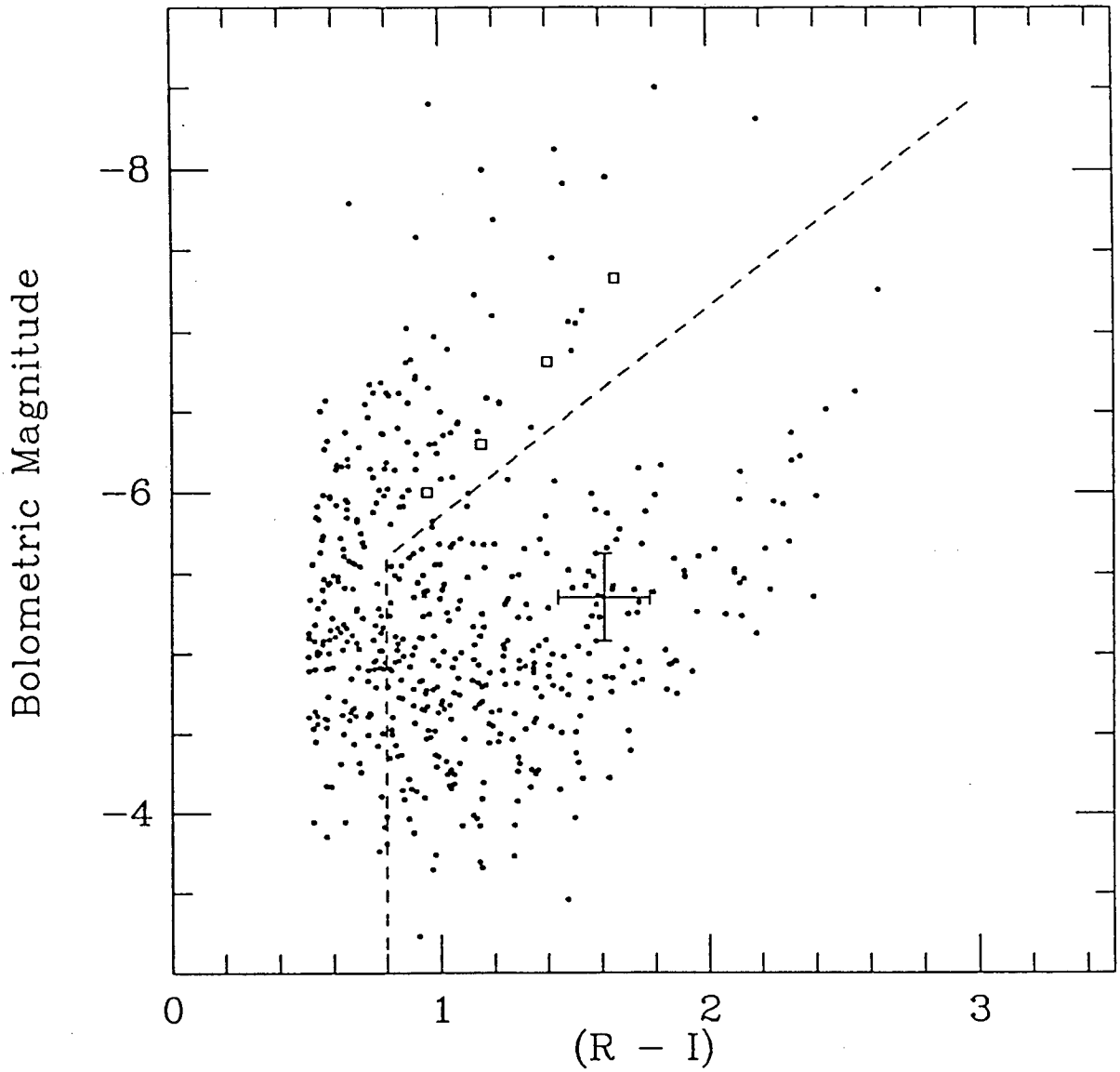


Figure 6: All stars redder than $(R - I) = 0.8$ and below the supergiant demarcation line are labelled as AGB stars. The open square are supergiants from Lee (1970). An error bar is also indicated.

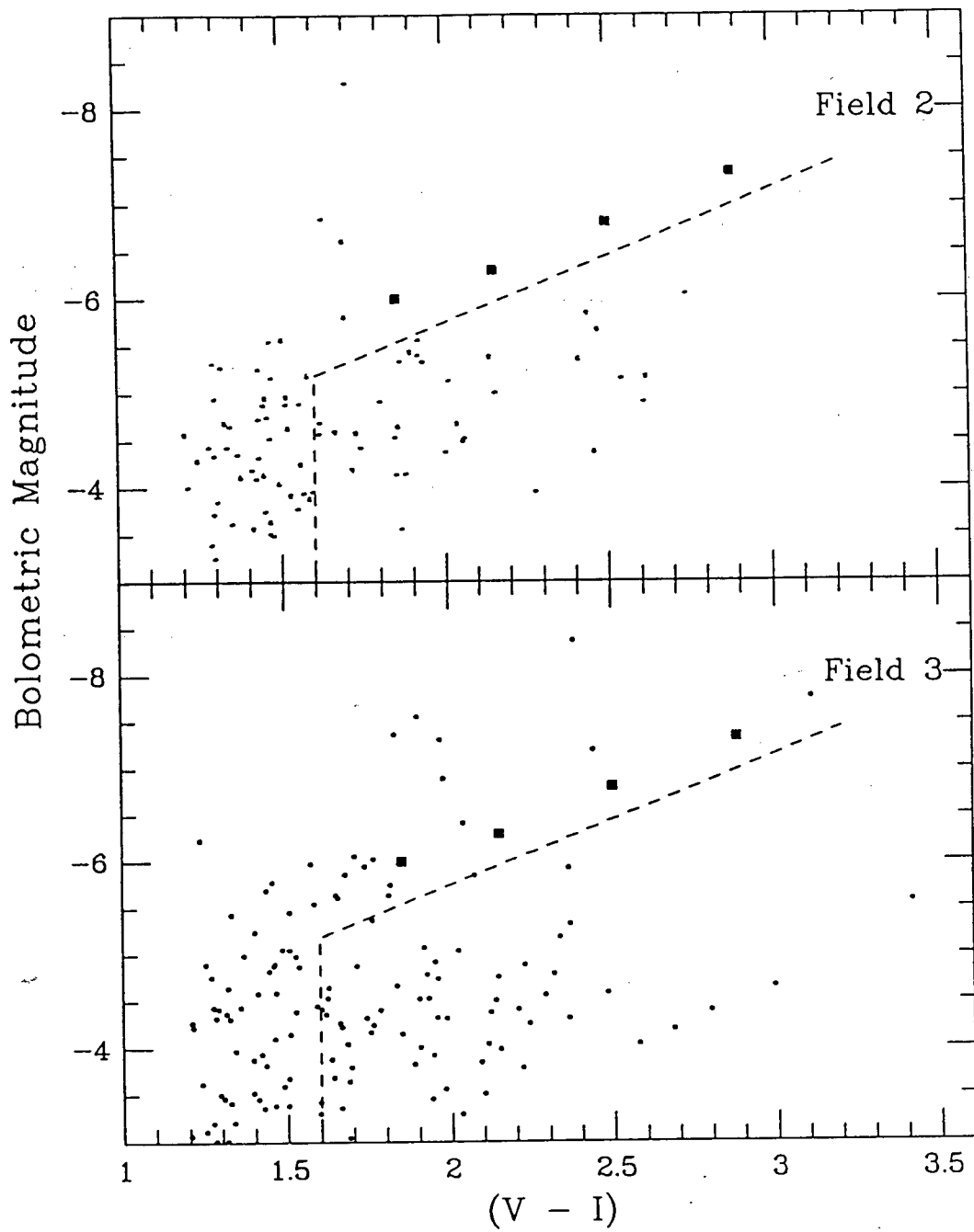


Figure 7: All stars redder than $(V - I) = 1.6$ and below the supergiant demarcation line are labelled as AGB stars.

4.3 Completeness and the Luminosity Function

The application of completeness corrections to determine a “true” luminosity function from an observed luminosity function is a non-trivial exercise. A recent paper by Mateo (1988) gives an excellent and thorough discussion of the many details involved. Completeness corrections for a bolometric luminosity function are further complicated by the presence of a color term in the bolometric correction (in this case, we have used a bolometric correction that has a quadratic color term, see equations 10 and 11). Since there is not a one-to-one correspondence between the I magnitude and the bolometric magnitude, we must include color data in the completeness tests.

To yield accurate completeness information, the artificial stars from the ADDSTAR tests should be treated in the same way as the program data. Thus, ADDSTAR frames were created in pairs (i,r or i,v) to accomplish three things: (1) to test the recovery rate of artificial stars as a function of color for each magnitude, (2) to test the efficiency of the routine which matches the star positions between the frames, and, (3) to allow the artificial stars to be calibrated, exactly as the program data. Also, the artificial stars were separated according to the dividing line of Figure 6 so that the corrections would apply directly to stars which fell within the AGB zone. In practice, stars that were recovered on only one of the two frames were not counted as a ‘double-recovery’ was required to determine a color.

The simplest way to determine the actual corrections is to take the magnitude and

color information for each artificial star pair and transform them into a bolometric magnitude. The numbers of added and recovered stars can then be sorted into bins in bolometric magnitude and the completeness fractions as a function of bolometric luminosity are obtained. In reality, the situation is more complicated, since the completeness within a bolometric bin can vary strongly with color. To account for this, the color-bolometric magnitude diagram was divided up into a grid of 0.33 magnitudes in M_{bol} by 0.6 magnitudes in color. The coarseness of the completeness fractions from one bin to the next was reduced by decreasing the width of the color bins to 0.2 magnitudes using 3 and 4 point interpolation. Figure 8 shows the resulting family of completeness curves. The completeness fraction ($\Lambda_{M(bol),(R-I)}$) for each color bin is plotted as a function of the bolometric magnitude. Thus, a vertical cut in the diagram (i.e., in bolometric magnitude) gives the completeness fraction of the bolometric magnitude as a function of color. The number of stars observed in each 0.5×0.2 magnitude bin were then corrected for incompleteness using $N_{corrected} = N_{observed} / (\Lambda_{M(bol),(R-I)})$ and the corrected numbers were binned in bolometric magnitude. This procedure effectively weights the observed number of stars according to the distribution with color.

The bolometric luminosity function for AGB stars in NGC 2403 was constructed using a prescription similar to that given in RM84. Specifically, the criteria for a star to be an AGB star is that it be redder and more luminous than the tip of the giant

branch of the metal-poor globular cluster M92, ie, $M_{bol} \leq -4.0$, and $(V - I) > 1.6$, or, from Bessell (1979), $(R - I) > 0.8$. AGB stars must also fall below the supergiant division lines discussed above.

The bolometric luminosity function, corrected for incompleteness, is tabulated in Table 4 and plotted in Figure 9 along with the luminosity function of the LMC from RM84 for comparison. The two functions are normalized to have the same total number of stars. A theoretical luminosity function computed in RM84 is also plotted in the figure. This curve represents the standard theoretical model with age 16 Gyr, a constant star formation rate (SFR), and an IMF slope of -2.35 (the ‘‘Salpeter’’ value).

The shape of the LMC luminosity function deserves some comment. The sample is large - more than 3000 stars - and complete so that the shape is not due to random or selection effects. Below $M_{bol} = -4.0$ we expect large numbers of first ascent giant branch stars, so the luminosity function is not expected to turnover at the faint end. The dip between $M_{bol} = -4.6$ and $M_{bol} = -6.5$ was identified by RM84 as a paucity of bright AGB stars. In a later study by Reid and Mould (1985), updated theoretical models were used along with a more complicated star formation history to obtain better agreement with the observed LMC luminosity function.

The NGC 2403 AGB luminosity function is clearly of a different shape than that of the LMC. Indeed, a test of χ^2 on the two luminosity functions has indicated, at

the 99.5 percentile, that the two distributions are drawn from different samples. This result remains even when the data points of the two functions are shifted together by one standard deviation. The following features of the NGC 2403 AGB luminosity function are noteworthy (cf. Figure 9). First, very few stars are seen in the brightest bolometric bins. These are also the reddest stars and many of them may have been missed due to the faint cutoff in the R filter. Second, there is good agreement with the theoretical function fainter than $M_{bol} = -5.6$; brighter than this, the observed function departs sharply from the theoretical function. Third, there is no evidence that bright AGB stars are ‘missing’ from this field in the sense inferred by RM84 for their LMC field. In fact, the NGC 2403 luminosity function appears to bulge out at approximately the same magnitude where the LMC luminosity function dips down. It is noted that scaling the NGC 2403 function up further at the faint end will not resolve the differences in the shape here. This may indicate that the NGC 2403 field has undergone a recent burst of star formation and the brighter stars have not yet evolved up to the AGB tip. The presence of HII regions in the field suggests that star formation may be ongoing.

A luminosity function has also been constructed for the stars of Fields 2 and 3. These are the outer disk fields and the two of them combined have fewer stars than Field 1 so they were corrected for incompleteness as above and put into bolometric bins of unit magnitude. The resulting function (see Table 4) is shown in Figure 10 again

with the LMC luminosity for comparison. The large bins and the small numbers of stars in the NGC 2403 fields prohibit detailed comparisons between the two luminosity functions. At the bright end, however, it is clear that the NGC 2403 fields have fewer luminous stars than the LMC. This is of concern because the field areas studied in the two different samples is comparable. Also, there are some supergiant candidates in each of the NGC 2403 fields, so we do expect some bright AGB stars as well (cf. Figure 6, Reid and Mould, 1985). The error bars in the figures have been determined from Equation 12 of Mateo (1988). The large error bars in the brightest bins of the NGC 2403 function are due to small number statistics.

The effects of the completeness corrections are shown in Figure 11. Here, both the corrected and uncorrected functions are plotted and it is seen that the shape of the uncorrected function has not been changed by the application of the completeness fractions. It should also be noted that reductions on the I and R frames were carried out with high star-finding thresholds so that contamination of the artificial star counts from noise spikes should be negligible.

Table 4: AGB Luminosity Functions

	M_{bol}	N_{obs}^a	N_{cor}^b	N_f^c	Error ^d
Field 1					
	-7.0 - -7.5	1	3	0.04	3
	-6.5 - -7.0	2	4	0.06	3
	-6.0 - -6.5	8	14	0.09	5
	-5.5 - -6.0	47	87	0.13	15
	-5.0 - -5.5	80	158	0.18	23
	-4.5 - -5.0	99	268	0.23	42
	-4.0 - -4.5	46	284	0.30	77
Fields 2 and 3					
	-6.0 - -7.0	1	1	0.10	1
	-5.0 - -6.0	21	28	0.22	6
	-4.0 - -5.0	54	115	0.63	23

^a N_{obs} = the number of stars observed.

^b N_{cor} = the number of stars corrected for completeness.

^c N_f = the number of foreground counts.

^dError is estimated by $\text{Error} = N_{\text{cor}} \sqrt{1/N_{\text{obs}} + 1/N_{\text{recovered}}}$, where $N_{\text{recovered}}$ is the number of artificial stars recovered in that bin.

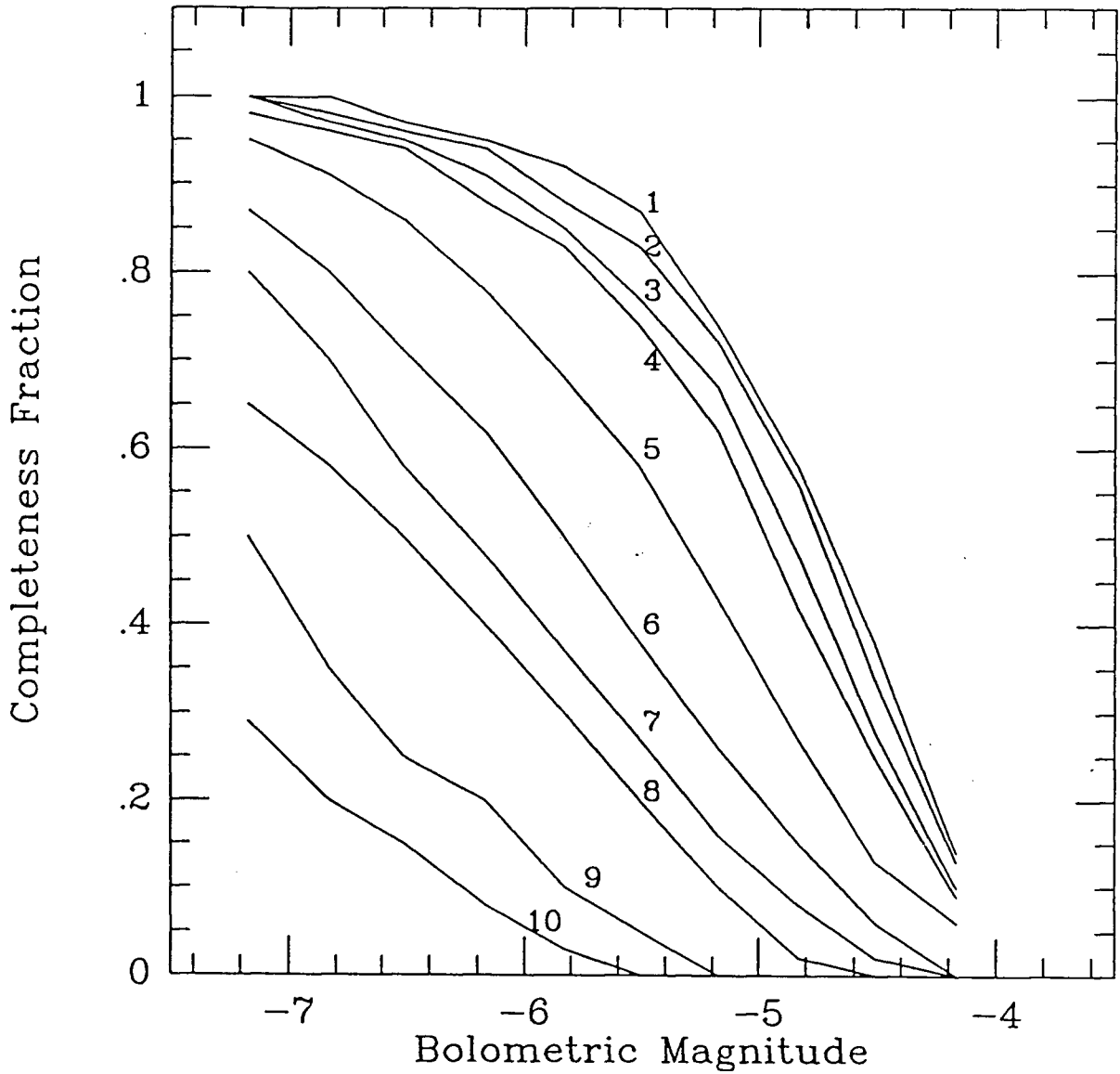


Figure 8: The completeness fraction as a function of bolometric magnitude for each color bin is shown. Curve 1 is for the color range $(R - I) = 0.8$ to 1.0 , Curve 2 is for the range 1.0 to 1.2 and Curve 10 is for the range 2.8 to 3.0 . A cut in bolometric magnitude gives the completeness fraction as a function of color for that magnitude.

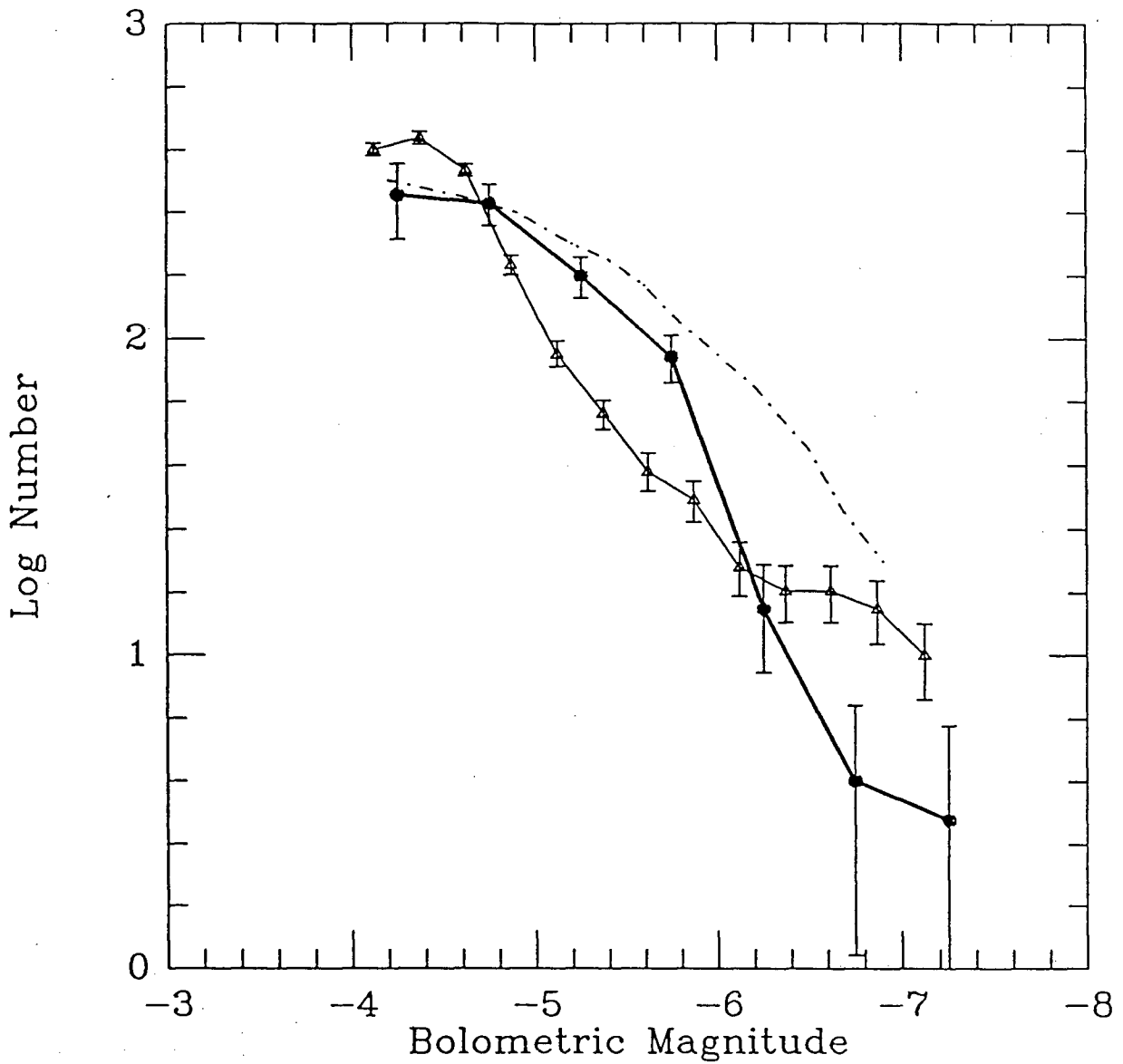


Figure 9: Luminosity Function: the heavy line of filled circles is the NGC 2403 function for Field 1 and the lighter line of filled triangles is the LMC function of RM84. The functions are scaled to the same total number of stars. The third curve represents a theoretical luminosity function with constant star formation from RM84. It is normalized to the NGC 2403 function at $M_{bol} = -4.75$.

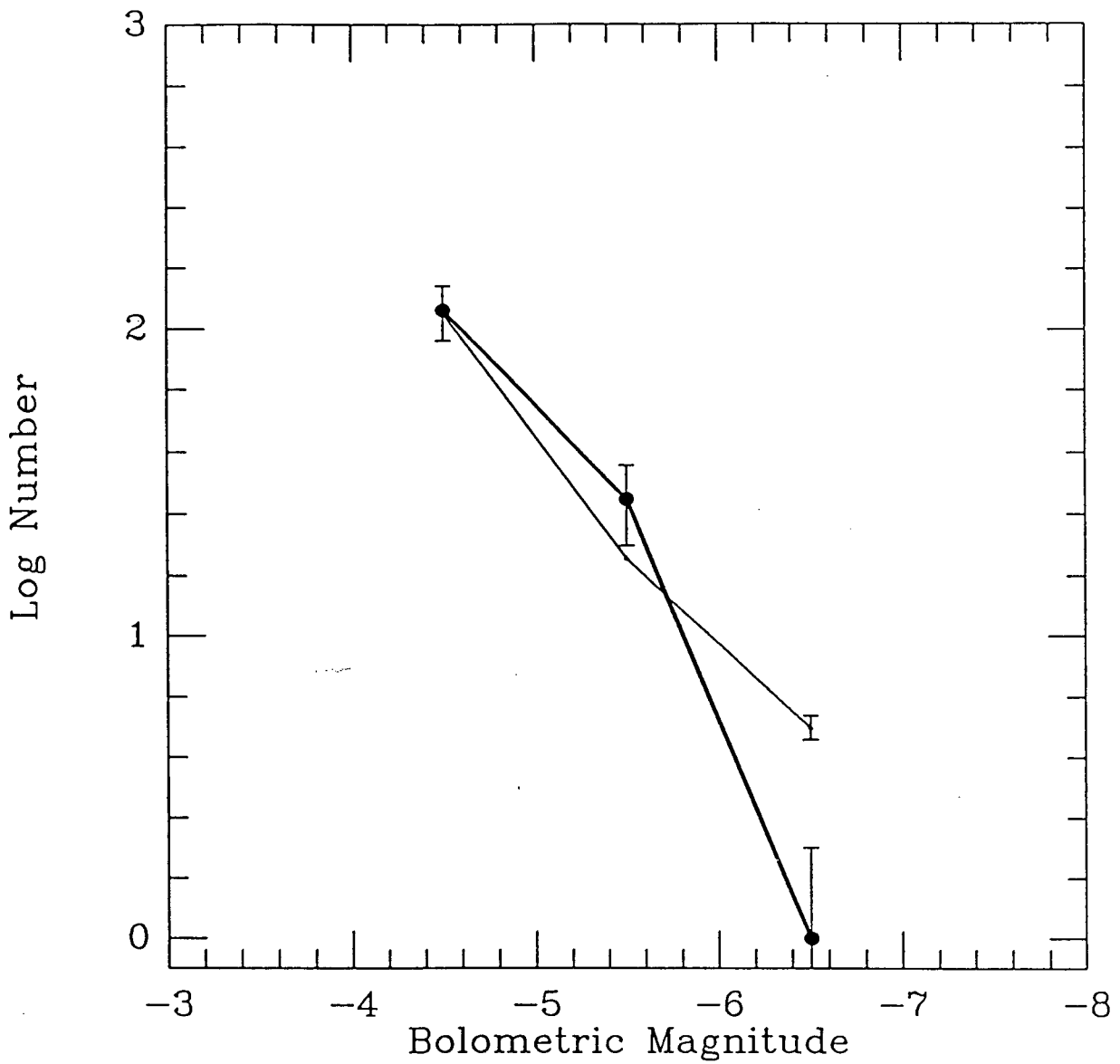


Figure 10: Luminosity Function: the heavy line of filled circles is the NGC 2403 function for Fields 2 and 3 and the lighter line is the LMC function of RM84 binned in unit magnitude.

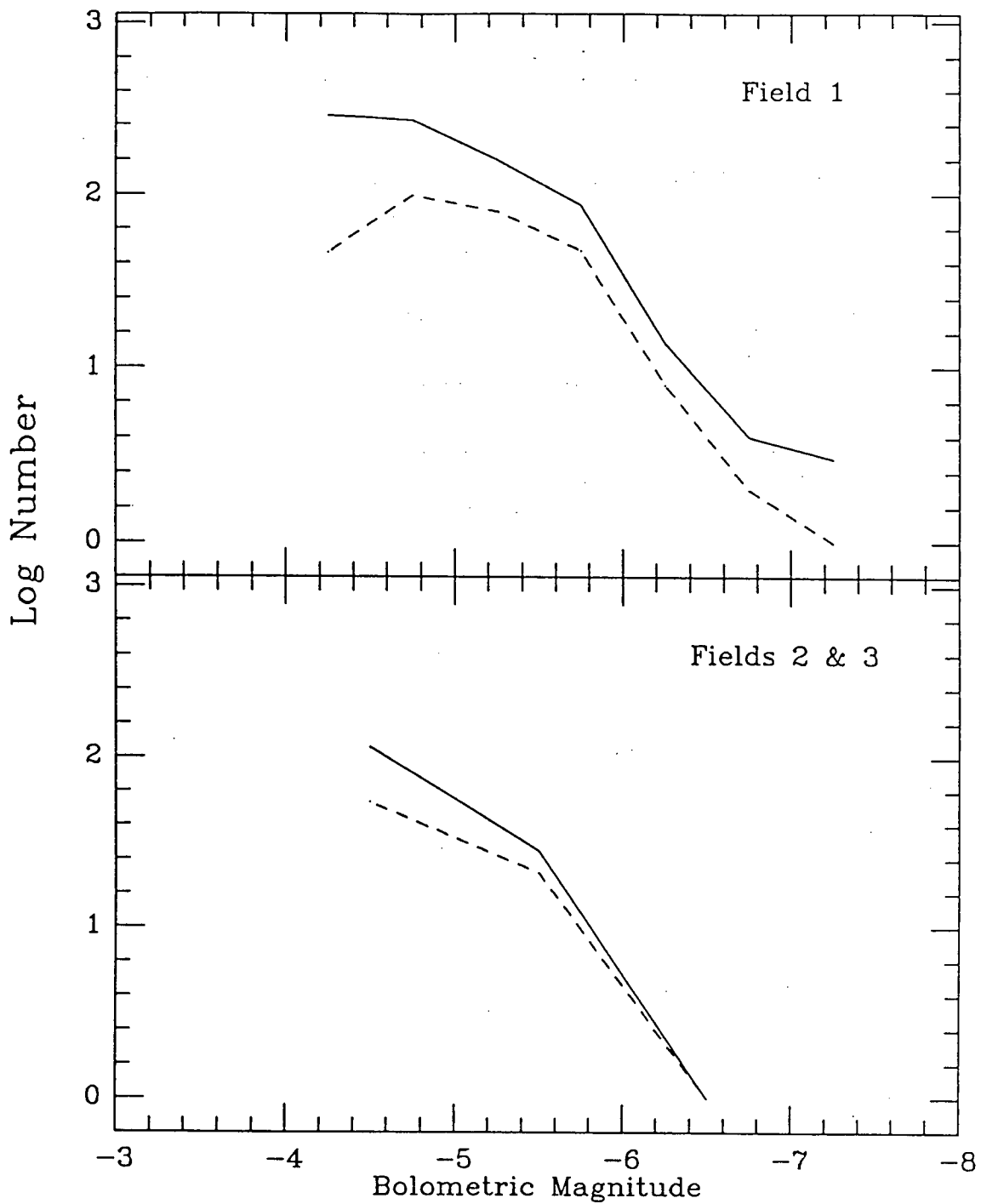


Figure 11: The solid line is the AGB luminosity function corrected for incompleteness and the dashed line is uncorrected. The completeness corrections do not change the shape of the luminosity function.

5 The Distance to NGC 2403

There have been several determinations of the distance to NGC 2403 based on Cepheid photometry over the past two decades. These are reviewed by Freedman and Madore (1988, hereafter FM88) where they also derive a new distance modulus of 27.51 ± 0.24 based on random-phase I-band observations of 10 known Cepheids. In this section, an independent distance modulus to NGC 2403 is derived from random-phase I-band observations of 4 Cepheids (see Table 5), which are in common with the sample of FM88.

The advantages of using long wavelengths for Cepheid observations are threefold: (1) the effects of reddening and metallicity are greatly reduced, (2) the amplitude of the light variation of a single Cepheid is much smaller, making estimates of mean luminosity more reliable and (3) the apparent luminosity width of the instability strip is decreased.

The procedure is simply to determine a period-luminosity (P-L) relation for Cepheids in a galaxy of known distance and then to force the NGC 2403 Cepheids to overlap so that the scatter is minimized. The difference in zero points (i.e., the shift in magnitude) gives the *relative* distance modulus between the calibrating galaxy (in this case, the LMC), and NGC 2403. The key assumption here is that the slope of the P-L relation for Cepheids in the two galaxies is the same.

First, the measured magnitudes of the Cepheids in each of the two galaxies must

be de-reddened. Differential reddening is not suspected to be significant for the LMC Cepheids (cf. Figure 4 of Martin, Warren and Feast (1979)) and this was confirmed by Caldwell and Coulson (1985) who found a low dispersion in the reddening of Cepheids in both Clouds. Thus, their value of $E(B - V)_{LMC} = 0.074$ was used. Reddening toward NGC 2403 was taken to be $E(B - V) = 0.06$ (Tammann and Sandage 1968). Using the extinction curve of Savage and Mathis (1979), these values transform to $A_I = 0.13$ and 0.10 , respectively.

Data for the LMC Cepheids were taken from Table 1 of Madore (1985) and it is assumed to be on the Cousins system. Following FM88, the distance modulus to the LMC is taken to be 18.50 ± 0.15 . The SMC can also be used as the calibrating galaxy although its decreased metallicity and greater depth along the line of sight (Feast 1986) compared to the LMC make it less suitable. However, it is still useful as a check on the results derived from the LMC Cepheids. The SMC data are from Table 3 of Madore (1985) and a reddening of $E(B - V)_{SMC} = 0.054$ is used (Caldwell and Coulson 1985).

Several distance estimates are obtained using both the present sample of 4 Cepheids alone and in combination with the FM88 sample. FM88 do not include Cepheids with periods in excess of $\log P = 1.8$ due to possible curvature in the P-L relation at the longest periods. It is interesting to note that this curvature is not observed in the SMC P-L relation. FM88 also neglected Cepheids with periods less than 10 days but

give no reason for this omission.

The results of this analysis are compiled in Table 6. There are three ranges in $\log P$: (1) $0.8 < \log P < 2.2$: all the stars in Table 1 of Madore (1985) with both V and $(V - I)$, (2) $0.8 < \log P < 1.8$: all but the longest period Cepheids, and (3) $1.0 < \log P < 1.8$: the same as FM88: neglecting Cepheids with the shortest and longest periods.

Taking the average of results from the shortest (range 3) and longest (range 1) range gives a relative distance between the LMC and NGC 2403 of 8.90 and a true distance modulus to NGC 2403 27.40. The dominant contributor to the error is the random error in the least squares fit of the LMC P-L relation which is 0.24 for range 1. The different ranges used in the P-L relation account for the slight difference in this distance and that determined by FM88. The P-L relation for the LMC Cepheids shifted to the distance of NGC 2403 is shown in Figure 12.

Table 5: Cepheid Observations in NGC 2403

Cepheid	log P	I mag. (error)
V 3	1.942	20.04 (0.01)
V 40	1.314	21.39 (0.04)
V 42	1.306	21.92 (0.07)
V 46	1.765	21.01 (0.03)

Table 6: Summary of P-L fits

Stars	log P	slope of P-L relation	Δ^a	$(m - M)_{2403}$
SMC				
4	0.8 - 2.2	-3.032	8.674	27.56
10	0.8 - 2.2	-3.032	8.593	27.48
LMC				
4	0.8 - 2.2	-2.808	8.974	27.47
3	0.8 - 1.8	-3.150	9.060	27.56
3	1.0 - 1.8	-3.430	9.047	27.55
10	0.8 - 2.2	-2.808	8.852	27.35
9	0.8 - 1.8	-3.150	8.930	27.43
9	1.0 - 1.8	-3.430	8.948	27.45
Adopted ^b			8.90	27.40

^aRelative distance modulus between NGC 2403 and the LMC or SMC

^bThis study.

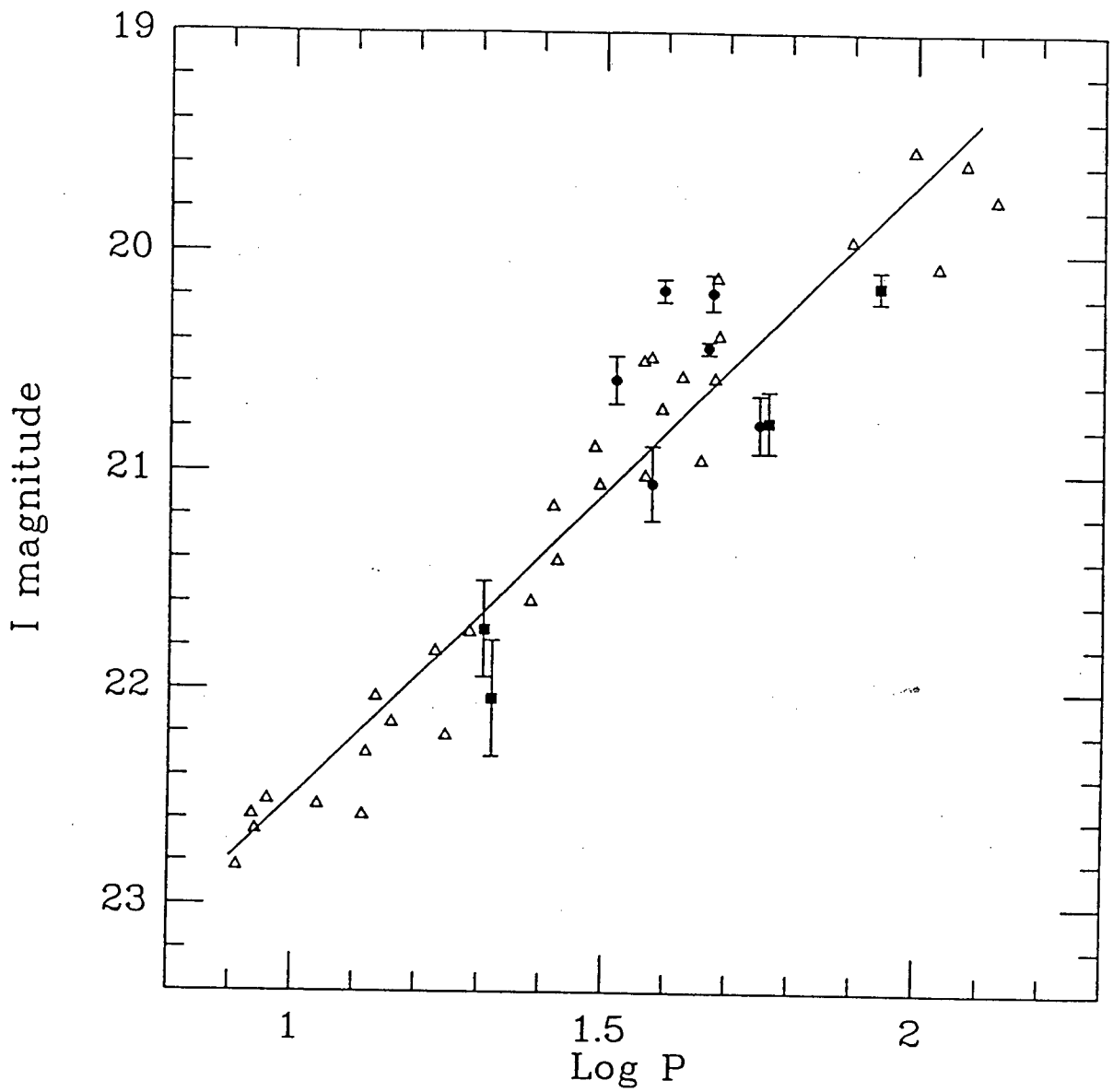


Figure 12: The 10 NGC 2403 Cepheids are the filled circles and squares, the squares are the independent observations from this study.

6 The C and M Star Study

6.1 The Photometric Method

A useful diagnostic in the study of late-type stellar populations is the C-to-M star number ratio. The C/M ratio has a strong correlation with metal abundance (cf. Figure 7, Pritchett *et al.* 1987). The competing explanations for the correlation are discussed by Richer (1988). To derive the C/M ratio, the two types of stars must first be distinguished. Thus, a simple narrowband photometric technique was developed by Richer (see Richer *et al.* 1984) and independently by Aaronson (CAN86) which exploits the differences in the spectra of C and M stars.

Figure 13 shows the placement of the narrowband filters in relation to the spectra of typical C and M stars, along with an F supergiant for comparison. The spectra were obtained by Grant Hill using the UBC 16 in. telescope and Reticon detector. Both the narrowband filters have bandwidths of approximately 200 Å. The "77" filter, centered at a wavelength of 7750 Å, falls on the TiO absorption band for M stars and on the continuum for C stars. The "81" filter, centered at 8100 Å, measures the CN absorption for C stars and the continuum for M stars. Thus, an index of "(81-78)" will be positive for C stars but negative for M stars. Stars of intermediate spectral type, like the F star, are insensitive to the (81-78) index, but the hottest stars, types O and B, have an index similar to that of carbon stars due to the slope of continuum at IR wavelengths. Therefore, an additional color, (R-I) or (V-I), is used to separate

the cool stars from the rest.

This method has been used successfully for several galaxies: NGC 55 (Pritchett *et al.* 1987), M31 (Richer and Crabtree 1985), NGC 300 (Richer, Pritchett and Crabtree 1985, hereafter RPC85), NGC 205 (Richer, Crabtree and Pritchett 1984) and several dwarf irregular galaxies (CAN86).

6.2 The Color-Color Diagram

The $(81 - 78)$ index versus $R - I$ color for the inner field of NGC 2403 is shown in Figure 14. Stars that have anomalously high errors for their magnitude bins, due to crowding and/or fitting errors (see Section 2), were omitted from the lists before the matching. A matching radius of 1.0 pixel was used so that only stars with well-determined positions, and hence low photometric errors, are included. This selection process left 140 stars for the plot. An increased matching radius results in greater scatter in the diagram.

The scatter in the $(81 - 78)$ index for the blue stars is almost 1.5 magnitudes, much worse than a comparable diagram for NGC 300 (Fig. 2 in RPC85) but similar to that of NGC 55 (Fig. 3 in Pritchett *et al.* 1987). There is still evidence, however, of a main band between $(R - I) = 0.0$ and 1.0 which then bifurcates near $(R - I) = 1.0$. Stars observed in the LMC (RPC85) with a similar filter system are superimposed as open circles and show a main band that splits into C stars with a high index and M

stars with a low or negative index at red colors. The filled circles are known C and M stars plus stars of earlier spectral type that were observed the same night as the Field 1 data. Figure 14 indicates that there are a handful each of C stars and a few more M stars in the program field. The C and M star zones, marked by the dashed lines, have been drawn using these known stars (circles) as a guide. Stars that fall in between these zones on the low side are likely K stars (CAN86) or possibly M stars with larger photometric errors.

For the 8 C star candidates, the mean color is $\overline{(R - I)} = 1.17 \pm 0.16$. Blanco, McCarthy and Blanco (1980) found $\overline{(R - I)} = 0.98$ for their sample of C stars in the SMC and $\overline{(R - I)} = 1.27$ for C stars in the LMC. Also, the 8 C star candidates seem to be split into two groups by magnitude. The first group, composed of the stars with high (81-78) indices plus one star with a low index but a very red color, has a mean I magnitude of 21.23 ± 0.14 , the second group is the remainder of the stars at the low edge of the zone and has a mean I magnitude of 20.56 ± 0.17 . Taken together the mean I magnitude for the 8 stars is 20.92 ± 0.37 .

If the NGC 2403 C stars are similar to those in the LMC (Richer 1981), the mean of the C star distribution is expected to be found at $I \sim 22.6$ (using a distance modulus of 27.4). The stars observed here have $M_I \lesssim -6.0$ and could represent the tip of the distribution but C stars have never been observed to be this bright in extragalactic systems. However, some C stars in galactic binary systems (Olson and Richer, 1975)

have been measured in this luminosity range. Since the peak of the C star distribution has not been observed in NGC 2403, it is not possible to estimate the distance to the galaxy using these C stars.

As mentioned earlier, the poor quality of the 8100 frame limits this study. The fainter group of potential C stars all have "81" magnitudes of ~ 24 where completeness is $\sim 10\%$ and the errors large.

There are 17 M star candidates in Figure 14. Thus, the C/M number ratio is 8/17. Hence, from the relation between the C/M ratio and $[Fe/H]$ given in Pritchett *et al.* (1987), we predict that the metallicity in this field of NGC 2403 is $[Fe/H] = -0.35$, a near-solar abundance and similar to that of NGC 300. To our knowledge, this is the first metallicity determination in NGC 2403. If some M stars are rejected as foreground stars, this value of the metallicity becomes more negative.

Table 7: C and M stars in NGC 2403

(X,Y)	I	(R - I)	(81 - 78)
C stars			
161,311	20.80(0.02)	1.09(0.05)	0.42(0.12)
101,220	20.48(0.02)	1.11(0.05)	0.44(0.09)
59,359	20.41(0.02)	1.28(0.04)	0.46(0.08)
130,303	20.55(0.02)	1.19(0.04)	0.49(0.07)
99,169	21.03(0.05)	1.50(0.08)	0.49(0.14)
298, 96	21.21(0.04)	1.10(0.06)	0.82(0.23)
75,242	21.33(0.07)	1.02(0.09)	0.87(0.18)
105,175	21.33(0.06)	1.04(0.09)	1.05(0.33)
M stars			
70,316	19.64(0.02)	1.49(0.03)	-0.05(0.05)
280,270	19.33(0.01)	1.71(0.02)	-0.05(0.03)
198, 18	19.00(0.03)	1.91(0.04)	-0.74(0.02)
149,275	19.78(0.01)	2.31(0.03)	-0.54(0.04)
206,328	21.63(0.05)	1.56(0.09)	-0.50(0.18)
159,337	21.23(0.04)	1.65(0.07)	-0.40(0.12)
111,260	21.40(0.06)	1.22(0.11)	-0.32(0.18)
109,157	21.35(0.05)	1.44(0.11)	-0.28(0.19)
40,230	22.21(0.09)	1.08(0.14)	-0.26(0.39)
21,239	20.09(0.01)	1.56(0.03)	-0.24(0.06)
120,436	21.67(0.07)	1.30(0.11)	-0.24(0.36)
56,320	20.06(0.02)	1.61(0.03)	-0.23(0.05)
127,197	18.98(0.01)	1.51(0.03)	-0.11(0.03)
215, 40	21.26(0.04)	1.84(0.08)	-0.20(0.18)
60,458	21.50(0.04)	1.90(0.11)	-0.15(0.21)
287,290	19.22(0.01)	1.54(0.02)	-0.17(0.03)
92,294	20.12(0.02)	1.59(0.04)	-0.19(0.06)

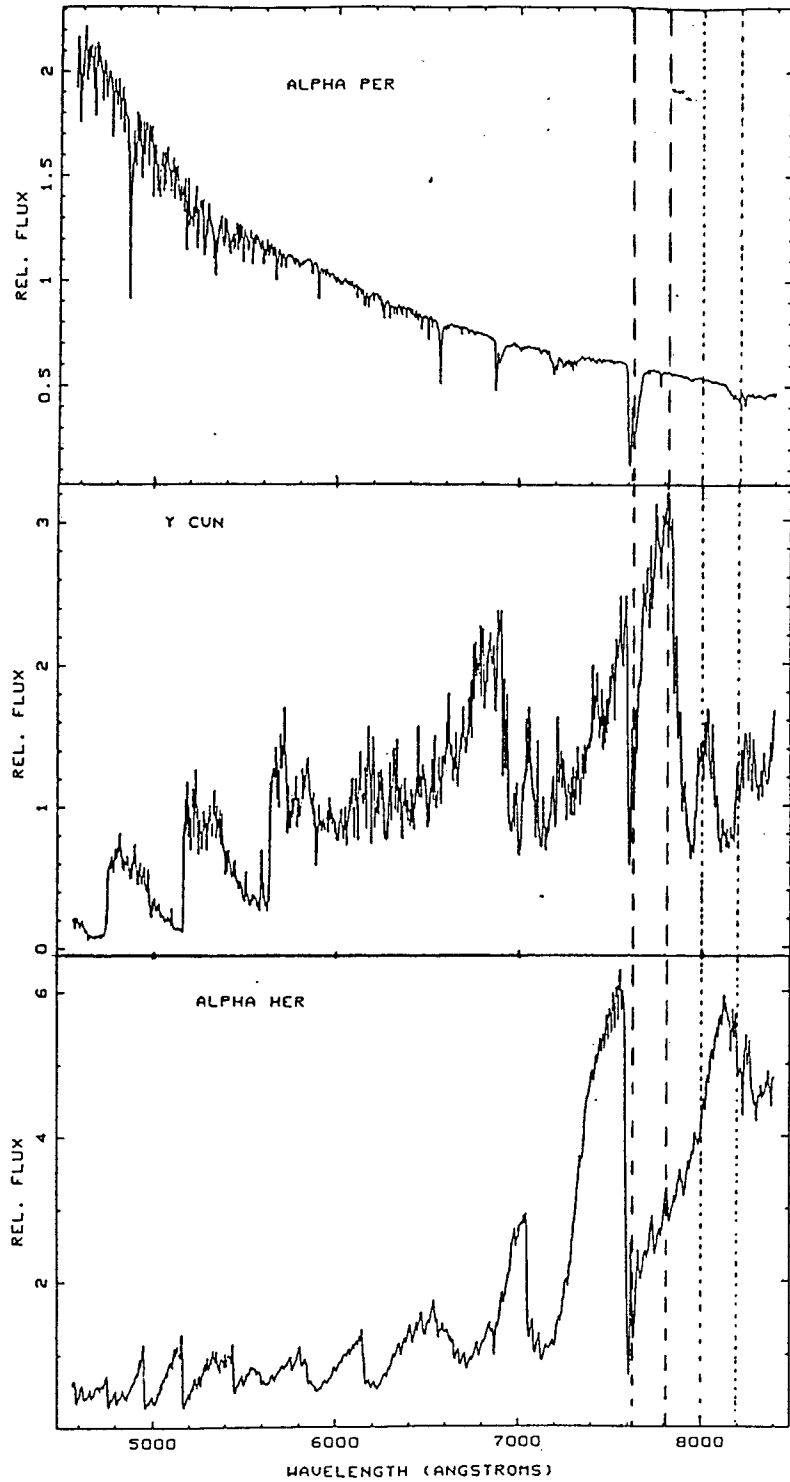


Figure 13: The placement of the narrowband filters on the spectra of an F star (Alpha Per), a C star (Y CVn) and an M star (Alpha Her) are shown.

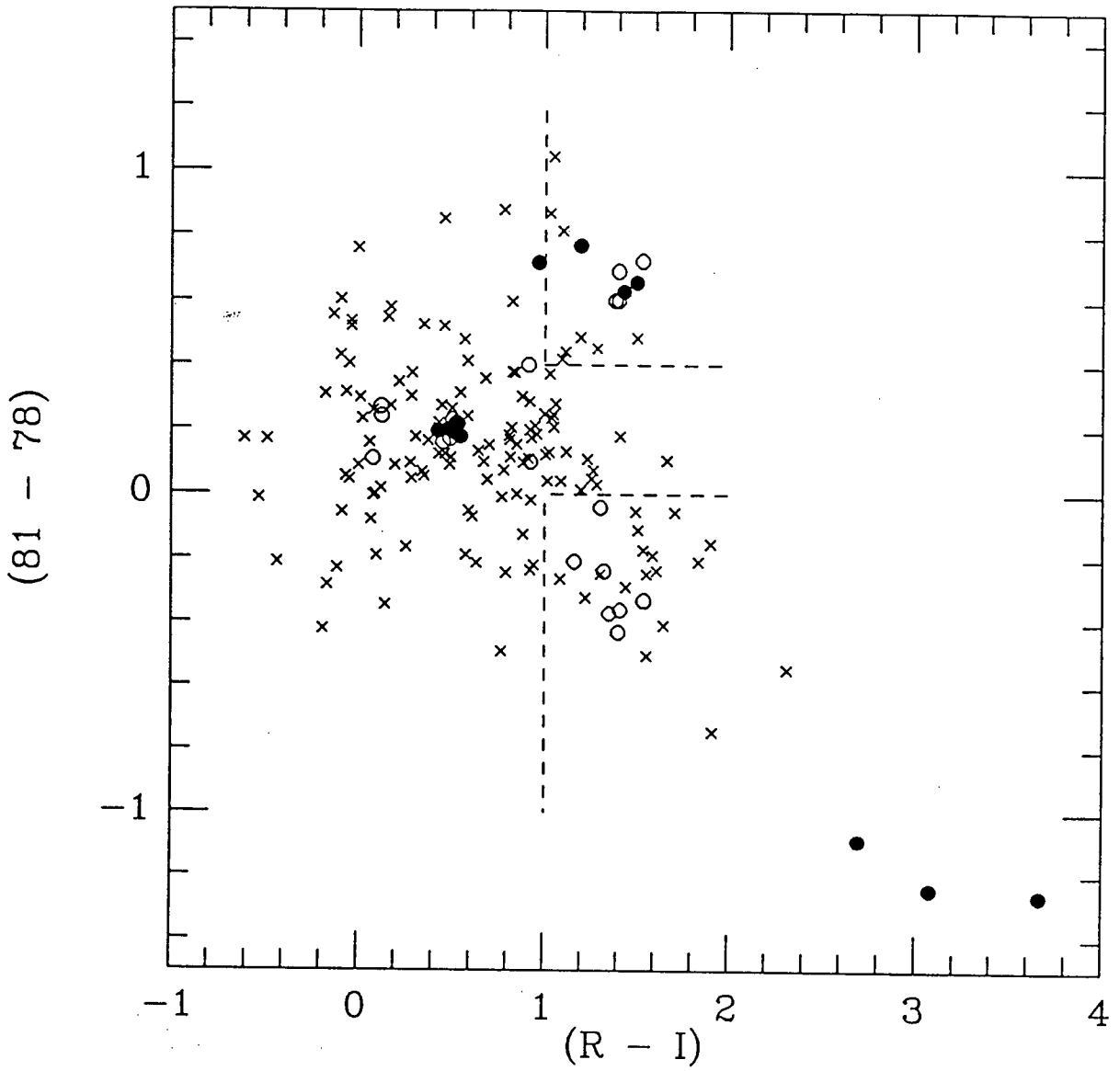


Figure 14: Filled circles are known galactic stars, open circles are LMC stars and x's are NGC 2403 stars.

7 Summary

The late-type stellar content of three disk fields of the galaxy NGC 2403 have been examined using CCD VRI photometry. A narrowband photometric technique has also been used to search for carbon and M stars in one of the fields. The major results are as follows:

1. A color-magnitude diagram for the innermost field revealed several red and blue supergiants.
2. The AGB luminosity function has been derived for each field, and compared with that for the LMC. As in the LMC, bright AGB stars are not found in the NGC 2403 in the numbers expected. It is argued that this effect is not due to incompleteness effects of the sample. The shape of the AGB luminosity function for the innermost field indicates that it may have undergone a recent burst of star formation. HII regions in the field suggest that is ongoing.
3. The distance to NGC 2403 has been derived from random phase I-band observations of a sample of 10 Cepheids. The true distance modulus obtained was 27.40 ± 0.24 ; the relative distance modulus between the LMC and NGC 2403 was 8.90.
4. A narrowband study identified several C and M star candidates. The metallicity was determined using a relation between C/M ratio and $[Fe/H]$. For the

innermost field, we found a C/M ratio of 8/17 and a near-solar metal abundance of $[Fe/H] = -0.35$. This is the first metallicity determination for NGC 2403.

Bibliography

- [1] Aaronson, M. 1983, in *Structure and Evolution of the Magellanic Clouds*, eds. S. van den Bergh and K.S. de Boer, (Dordrecht: Reidel), p. 183.
- [2] Aaronson, M. 1986, in *Stellar Populations*, eds. Colin A. Norman, Alvio Renzini and Monica Tosi, (Cambridge:Cambridge University Press), p. 45.
- [3] Bahcall, J., Casertano, S. and Ratnatunga, K.U. 1987, *Ap. J.*, **320**, 515.
- [4] Bessell, M.S. 1979, *P.A.S.P.*, **91**, 589.
- [5] Bessell, M.S., and Wood, P.R. 1984, *P.A.S.P.*, **96**, 247.
- [6] Blanco, V.M., McCarthy, M.F. and Blanco, B.M. 1980, *Ap. J.*, **242**, 938.
- [7] Caldwell, J.A.R., and Coulson, I.M. 1985, *M.N.R.A.S.*, **212**, 879.
- [8] Chiosi, C. 1986, in *Spectral Evolution of Galaxies*, eds. C. Chiosi and A. Renzini, (Dordrecht: Reidel), p. 237.
- [9] Christian, C.A., Adams, M., Barnes, J.V., Butcher, H., Hayes, D.S., Mould, J.R., Siegel, M. 1985, *P.A.S.P.*, **97**, 363.
- [10] Cook, K.M., Aaronson, M. and Norris, J. 1986, *Ap. J.*, **305**, 634 (CAN86).
- [11] Drukier, G.A., Fahlman, G.G., Richer, H.B., and Vandenberg, D.A. 1988, *A.J.*, **95**, 1415.
- [12] Feast, M.W. 1986, in *Galaxy Distances and Deviations from Universal Expansion*, eds. B.F. Madore and R.B. Tully, (Dordrecht: Reidel), p. 7.
- [13] Freedman, W.L., and Madore, B.F. 1988, preprint (FM88).
- [14] Frogel, J.A., Cohen, J.G., Persson, S.E. and Elias, J.H. 1981, in *Physical Processes in Red Giants*, eds. I. Iben and A. Renzini, (Dordrecht: Reidel), p. 159.
- [15] Grieve, G.R. 1984, in *LIPS Manual*, unpublished.

- [16] Hendon, A.A. and Kaitchuck, R.H. 1982, in *Astronomical Photometry*, (New York: Van Nostrand Reinhold).
- [17] Humphreys, R.M. 1986, *A. J.*, **91**, 808.
- [18] Iben, I. 1981, *Ap. J.*, **246**, 278.
- [19] Iben, I. 1983, in *Observational Tests of the Stellar Evolution Theory*, eds. A. Maeder and A. Renzini, (Dordrecht: Reidel), p. 3.
- [20] Lattanzio, J.C. 1988, in *Evolution of Peculiar Red Giant Stars*, in press.
- [21] Lee, T.A. 1970, *Ap. J.*, **162**, 217.
- [22] Madore, B.F. 1985, in *I.A.U. Colloquium No. 82, Cepheids: Theory and Observations*, ed. B.F. Madore, (Cambridge: Cambridge University Press), p. 166.
- [23] Martin, W.L., Warren, P.R. and Feast, M.W. 1979, *M.N.R.A.S.* **188**, 139.
- [24] Mateo, M. 1988, *Ap. J.*, **331**, 261.
- [25] Mould, J. 1983, in *Structure and Evolution of the Magellanic Clouds*, eds. S. van den Bergh and K.S. de Boer, (Dordrecht: Reidel), p. 195.
- [26] Mould, J.R., Kristian, J. and Da Costa, G.S. 1983, *Ap. J.*, **270**, 471.
- [27] Olson, B.E. and Richer, H. 1975, *Ap. J.*, **200**, 88.
- [28] Pritchett, C.J., Richer, H.B., Schade, D.S., Crabtree, D. and Yee, H.K.C. 1987, *Ap. J.*, **323**, 79.
- [29] Ratnatunga, K. 1988, private communication.
- [30] Reid, N. and Mould, J. 1984, *Ap. J.* **284**, 98 (RM84).
- [31] Reid, N. and Mould, J. 1985, *Ap. J.* **299**, 236.
- [32] Reid, N., Mould, J. and Thompson, I. 1987, *Ap. J.*, **323**, 433.
- [33] Richer, H.B. 1981, in *Physical Processes in Red Giants*, eds. I. Iben and A. Renzini, (Dordrecht: Reidel), p. 153.

- [34] Richer, H.B. 1988, in *Evolution of Peculiar Red Giant Stars*, in press.
- [35] Richer, H.B. and Crabtree, D.R. 1985, *Ap. J.*, **298**, L13.
- [36] Richer, H.B., Crabtree, D.R. and Pritchett, C.J. 1984, *Ap. J.* **287**, 138.
- [37] Richer, H.B., Pritchett, C.J., Crabtree, D. 1985, *Ap. J.* **298**, 240.
- [38] Sandage, A. 1984, *A. J.*, **89**, 630.
- [39] Sandage, A. and Tammann, G. 1981, *A Revised Shapley-Ames Catalog of Bright Galaxies*, (Washington, D.C.: Carnegie Institution).
- [40] Savage, B.D. and Mathis, J.S. 1979, *Ann. Rev. Astr. Ap.* **17**, 73.
- [41] Schild, R.E. 1983, *P.A.S.P.*, **95**, 1021.
- [42] Stetson, P.B. 1987, *P.A.S.P.*, **99**, 191.
- [43] Stetson, P.B. and Harris W. 1988, preprint.
- [44] Tammann, G. and Sandage, A. 1968, *Ap. J.* **151**, 825.
- [45] Wood, P.R., Bessell, M.S. and Fox, M.W. 1983 *Ap. J.*, **272**, 99.
- [46] Walker, G.A.H. 1987, *Astronomical Observations: An Optical Perspective*, (Cambridge: Cambridge University Press), p. 306.